Thin Solid Films 595 (2015) 209–213

Contents lists available at ScienceDirect

Thin Solid Films

journal homepage: www.elsevier.com/locate/tsf

Thermal oxidation of Zr–Cu–Al–Ni amorphous metal thin films

R.P. Oleksak [a], E.B. Hostetler [a], B.T. Flynn [a], J.M. McGlone [b], N.P. Landau [b], J.F. Wager [b], W.F. Stickle [c], G.S. Herman [a,*]

[a] School of Chemical, Biological and Environmental Engineering, Oregon State University, Corvallis, OR 97331, United States
[b] School of Electrical Engineering and Computer Science, Oregon State University, Corvallis, OR 97331, United States
[c] Hewlett-Packard Company, Corvallis, OR 97333, United States

ARTICLE INFO

Article history:
Received 29 April 2015
Received in revised form 11 September 2015
Accepted 30 October 2015
Available online 10 November 2015

Keywords:
Amorphous metal thin film
Zr–Cu–Al–Ni
Thermal oxidation

ABSTRACT

The initial stages of thermal oxidation for Zr–Cu–Al–Ni amorphous metal thin films were investigated using X-ray photoelectron spectroscopy, transmission electron microscopy and energy dispersive X-ray spectroscopy. The as-deposited films had oxygen incorporated during sputter deposition, which helped to stabilize the amorphous phase. After annealing in air at 300 °C for short times (5 min) this oxygen was found to segregate to the surface or buried interface. Annealing at 300 °C for longer times leads to significant composition variation in both vertical and lateral directions, and formation of a surface oxide layer that consists primarily of Zr and Al oxides. Surface oxide formation was initially limited by back-diffusion of Cu and Ni (<30 min), and then by outward diffusion of Zr (>30 min). The oxidation properties are largely consistent with previous observations of Zr–Cu–Al–Ni metallic glasses, however some discrepancies were observed which could be explained by the unique sample geometry of the amorphous metal thin films.

1. Introduction

Bulk amorphous metals (i.e., bulk metallic glasses, BMGs) have been extensively investigated over the last 50 years [1]. In particular, Zr–Cu-based BMGs such as Zr–Cu–Al–Ni (ZCAN) have attracted significant interest due to their good glass forming ability, high mechanical strength and corrosion resistance [1,2]. More recently, amorphous metal thin films (AMTFs) have been shown to have potential as a replacement for polycrystalline thin films for a wide range of applications [3]. ZCAN is among the most thoroughly investigated AMTFs for applications such as nanoscale patterning [4,5], mechanical coatings [6], nanolaminates [7,8] and metal-insulator-metal devices [9,10].

Understanding the thermal oxidation of these materials is critical for the aforementioned and other potential applications. For example, the deposition of dielectric layers for metal-insulator-metal (MIM) devices often requires temperatures > 300 °C [9], and many other applications require similar thermal processes. The oxidation of AMTFs may either improve or degrade the materials properties. For example, while oxidation may be unfavorable for microelectronic applications where low resistivity and a well-defined interface are required, it may be desirable as a passivation layer for biomedical devices, which is an emerging application for both bulk [11] and thin film [12] amorphous metals. Although significant research has been conducted to better understand the oxidation of ZCAN as a BMG, these studies are largely limited to long annealing times at high temperatures which allows significant diffusion of all metal species. Understanding the initial oxidation (and associated composition variation) of AMTFs such as ZCAN [13] has received considerably less attention and is expected to be of interest to the scientific community at large.

In addition to thermal oxidation, the role of small quantities of oxygen incorporated during the material synthesis has been studied for many amorphous metals, including ZCAN in both thin film [14] and bulk [2,15] forms, and incorporation of oxygen has been shown to have significant effects on both structural and physical material properties [16]. Thus, the thermal stability of oxygen in these films has implications related to the processing requirements for many applications.

In this study the thermal oxidation of amorphous oxygen-containing ZCAN thin films was investigated using X-ray photoelectron spectroscopy (XPS), transmission electron microscopy (TEM) and energy-dispersive X-ray spectroscopy (EDS). Our results provide insight into the initial stages of thermal oxidation for ZCAN thin films during a 300 °C anneal in air.

2. Experimental details

ZCAN thin films (≈50 nm thick) were deposited onto thermally oxidized Si wafers (SiO_2 thickness ≈ 140 nm) and SiN windows (for top-down TEM analysis). DC magnetron sputtering was used to deposit the ZCAN films using a 3-in. $Zr_{40}Cu_{35}Al_{15}Ni_{10}$ target (Kamis Incorporated), a power of 60 W, a pressure of 3 mTorr, an Ar flow rate of 20 sccm, and a target to substrate distance of 4 in. The as-deposited samples were thermally oxidized in air using a tube furnace. The samples were inserted into a tube furnace held at the target temperature. After oxidation at

* Corresponding author at: 102 Gleeson Hall, Corvallis, OR 97331-2702, United States.
E-mail address: greg.herman@oregonstate.edu (G.S. Herman).

http://dx.doi.org/10.1016/j.tsf.2015.10.080
0040-6090/

the desired conditions (5, 15, 30, 60 and 120 min at 300 °C and 60 min at 400 °C) the samples were removed and allowed to cool to room temperature.

An FEI 80–200 kV Titan Scanning/Transmission Electron Microscope (S/TEM) operating at 200 kV with ChemiSTEM energy dispersive X-ray spectroscopy (EDS) was used for TEM analysis. Samples were prepared by depositing the films directly onto TEM grids with ≈20 nm thick SiN windows, or fabricated as thin film lift outs using a focused ion beam (FIB) in an FEI 3D DualBeam Scanning Electron Microscope. EDS line scans were collected with a step size between 1 and 2 nm and the data was averaged over 5 points to reduce noise.

XPS measurements were performed with a PHI Quantera Scanning ESCA system using monochromatic Al K_α radiation with a 100 μm spot size. The data were acquired with a 45° emission angle and an electron analyzer pass energy of 140 eV for the sputter depth profile data. The energy scale of the spectrometer is calibrated to Au $4f_{7/2}$ at 84.0 eV and Cu $2p_{3/2}$ at 932.7 eV. The sputter depth profiles were acquired by alternately sputtering the sample and then acquiring high resolution data at each sputter cycle. A monoatomic 2 kV Ar^+ ion beam rastered over a 2×2 mm^2 area was used for ion milling. XPS sputter times were adjusted to approximate depths by correlating to TEM cross-sectional images of films annealed at 300 °C for 60 min, where approximate sputter rates were determined separately for the metal film and the surface oxide. Quantification calculations were made using PHI MultiPak which incorporates established sensitivity factors corrected for the transmission function of the analyzer and the reported values should be regarded as semi-quantitative. Chemical state resolved depth profile analysis was performed by fitting the Zr *3d* spectra into both metallic (Zr-metal) and oxide (Zr-oxide) components at each sputter cycle. The quantification of the sputter depth profiles does not take into account effects of preferential sputtering.

3. Results and discussion

Plan-view TEM analysis of ZCAN films as-deposited and after a 300 °C, 60 min anneal is shown in Fig. 1. A high-resolution bright field (HRTEM) image of the as-deposited film is shown in Fig. 1a. The salt-and-pepper pattern and the lack of long range order suggest that the films are amorphous, consistent with previous studies [9]. A high-angle annular dark field (HAADF) image of the as-deposited film is shown in Fig. 1b, and reveals high electron density (light contrast) regions on the order of 10 nm surrounded by low electron density (dark contrast) regions. The short-range inhomogeneities observed in this low resolution HAADF image may be due to slight porosity in the film structure or segregation of low electron density elements (e.g., oxygen) to the boundaries of metal clusters. EDS analysis of this as-deposited film (data not shown) revealed a uniform 2-dimensional composition of all metal species within the spatial resolution of the technique. Fig. 1c shows a HAADF image of the ZCAN film after annealing to 300 °C for 60 min in air. These annealing conditions resulted in reduction in the clustering seen in the as-deposited sample and the development of significant long-range inhomogeneities. These inhomogeneities are seen as light and dark regions ranging from ≈10 to 100 nm that are dispersed throughout the ZCAN film. To gain insight into possible compositional variation between the dark and light regions, in Fig. 1d we show image contrast EDS data along the dashed line shown in Fig. 1c. The line scan suggests that the dark regions in the 300 °C annealed film represent oxygen-rich regions as indicated by peaks in O concentration near line distances of 40, 135, 280 and 390 nm. These regions also have a significant reduction in Cu content and a slight reduction in Ni content, suggesting these regions are composed primarily of Zr- and Al-oxides. The EDS line scan also includes a region of light contrast centered near the line distance of 300 nm. No significant change in composition is observed through this regime suggesting the lighter contrast is likely due to an increase in film thickness. Thus, thickness variation is introduced during the 300 °C anneal. It should be noted that the Cu concentration measured by EDS for this analysis was artificially increased via scattering effects from Cu present in the TEM specimen holder, however this does not affect the trends observed in the line scan.

In order to investigate the cross-sectional variation in structure and composition of annealed films both TEM cross-sections, EDS line scans, and XPS sputter depth profiles were performed and are shown in Fig. 2a, b and c, respectively. From right to left, the bright field TEM image shown in Fig. 2a consists of thermally oxidized SiO_2 which was grown on a Si substrate, ZCAN film annealed at 300 °C for 60 min, and amorphous carbon protective layers used to prevent sample damage during the FIB process. As seen in Fig. 2a, the ZCAN film lacks evidence of crystalline domains suggesting that the film remains amorphous after a 300 °C anneal in air. Cross-sectional electron diffraction measurements (data not shown) also confirmed that the films remain amorphous after this annealing process. The film appears laterally uniform with a low electron density surface layer ≈20 nm thick. Some degree of surface roughness leading to thickness variation is observed, consistent with our interpretation of the lighter contrast regions in plan-view HAADF analysis (Fig. 1c). An EDS line scan taken along the film cross-section and aligned to the image in Fig. 2a is shown in Fig. 2b. This line scan confirms the observed surface layer can be attributed to oxide formation. The oxide surface layer also has an increase in Zr and Al concentration and a decrease in Cu and Ni concentration, which is consistent with the lateral variation observed in Fig. 1d. These results suggest that a layer consisting primarily of Zr- and Al-oxides is formed at the film surface during the anneal. The increase in Zr- and Al-oxides after annealing in air at 300 °C is in agreement with previous studies of air oxidation of ZCAN BMG, while the lack of Cu-oxide observed at the surface is consistent with some previous studies [17] and not others [18]. In addition, two distinct regions of Cu- and Ni-enrichment are seen near the interface of the oxide layer and the ZCAN film at depths of 23 and 30 nm, respectively. An XPS depth profile of the same sample is shown in Fig. 2c and has a similar trend in composition throughout the film thickness,

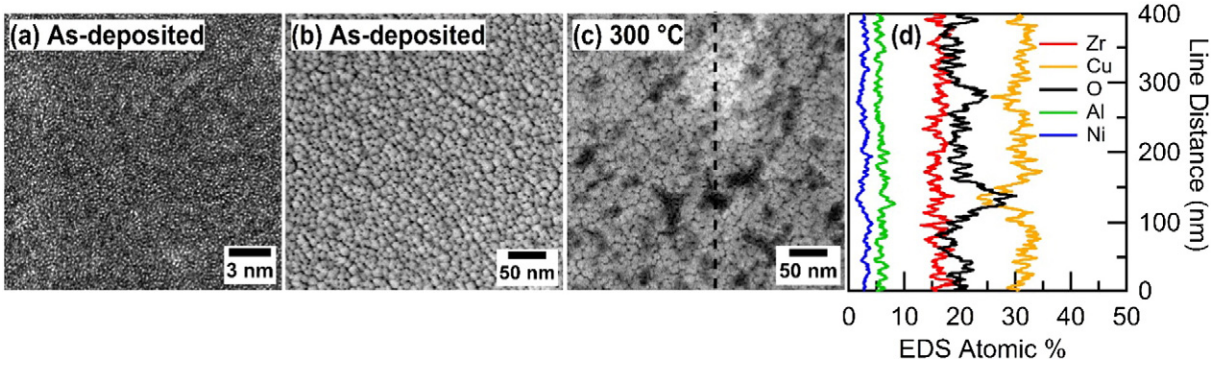

Fig. 1. Plan-view TEM analysis of ZCAN thin films. (a) HRTEM image of as-deposited film. (b) HAADF image of as-deposited film. (c) HAADF image of film annealed at 300 °C for 60 min. (d) EDS line scan taken across dashed line shown in (c).

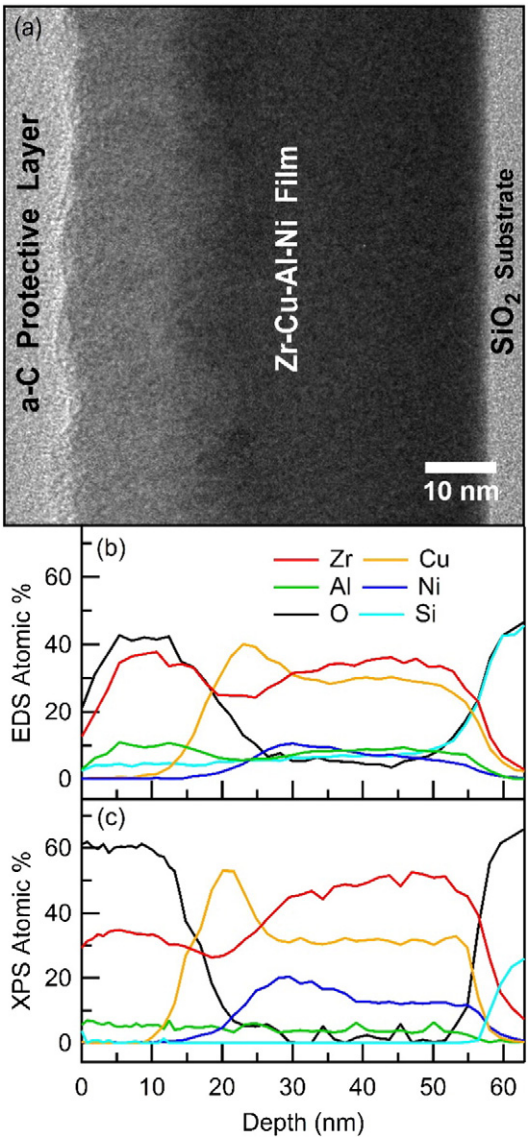

Fig. 2. Cross-sectional analysis of ZCAN thin film annealed at 300 °C for 60 min. (a) BFTEM image. (b) EDS line scan aligned to image shown in (a). (c) XPS depth profile aligned to image shown in (a).

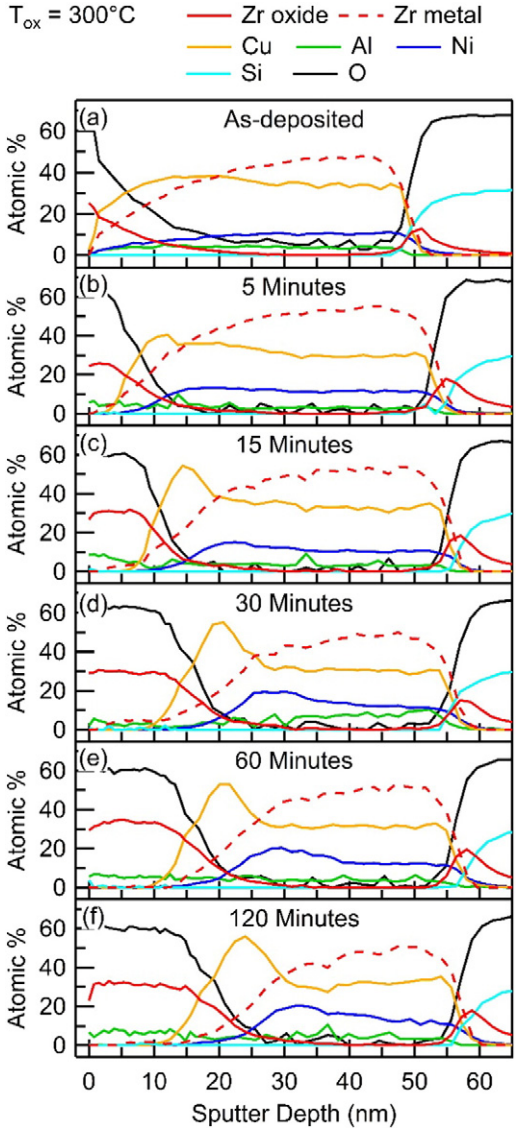

Fig. 3. XPS depth profiles of ZCAN thin films annealed at 300 °C.

where the primary differences are better-defined Cu- and Ni-rich regions and decreased variation in Al throughout the thickness of the film. A thin layer of lighter contrast observed in the BFTEM image (Fig. 2a) at the SiO_2 interface and the tailing of Zr signal into the SiO_2 interface suggests an oxide layer forms at the interface between the ZCAN film and the SiO_2 layer, which is consistent with a previous report [13].

To gain insight into the changes that occur during the annealing process chemical state resolved XPS sputter depth profiles are shown in Fig. 3 for an as-deposited sample and samples annealed to 300 °C for different times. The as-deposited film (Fig. 3a) is seen to have a relatively uniform distribution of metals, with a slight increase in Zr-metal and Ni for increasing depth into the film, which is accompanied by a slight decrease in Cu in the same region. A surface native oxide is present as indicated by the increase in the O and Zr-oxide signals at the surface [19]. A small amount of oxygen, incorporated during film deposition, is also observed throughout the film thickness. The atomic composition of the bulk of the films was estimated using the average concentration value obtained for the region just after etching through the surface oxide and just before etching through the substrate. For the as-deposited film the atomic composition was found to be approximately 47 at.% Zr, 32 at.% Cu, 5 at.% Al, 11 at.% Ni, and 5 at.% O. Previous samples deposited under the same conditions better matched the original target composition, suggesting preferential sputtering of the target over time may have caused a reduction in Al content [8]. The as-deposited film oxygen concentration was estimated to be 5 at.%, while after annealing at 300 °C for 5 min (Fig. 3b) the oxygen signal decreased throughout the film thickness to 2 at.%. These data suggest that the incorporated oxygen readily diffuses from the bulk of the film even during the initial stages of annealing. Little change of the oxygen content (1.6 ± 0.6 at.%) in the bulk of the ZCAN thin film was observed with additional annealing from 15 to 120 min.

In addition to oxygen diffusion from the bulk of the film we found that Cu and Ni segregation occurs at the interface of the oxide layer and metal ZCAN film, which leads to the onset of the Cu- and Ni-rich regions that were also observed in the 60 min anneal film cross-section and XPS sputter depth profiles (Fig. 2). The diffusion of Ni and Cu metal to the oxide interface was previously observed during the oxidation of ZCAN BMG [20]. In the present study, similar phenomena are observed, however the thin film geometry (i.e., the lack of a semi-infinite sink for Cu and Ni present in the BMG) results in an enrichment of these species at the oxide interface. This trend continues for increased annealing times (Fig. 3c–f), where Cu- and Ni-rich regions segregate further into the film during growth of the Zr- and Al-oxide surface

layer. This process is summarized in Fig. 4. As seen in Fig. 4a, the maximum Cu concentration increases from 38.5 to 54.3 at.% from 5 to 15 min, with little variation (53.0–56.0 at.%) for additional annealing time. An increase in maximum Ni concentration is much more gradual, where the maximum concentration increases from 11.1 to 19.5 at.% from 5 to 30 min, with minimal increase (<1 at.%) between 30 and 120 min annealing time. As seen in Fig. 4b, the location of the Cu-rich and Ni-rich zones relative to the growing surface oxide remain relatively constant with increasing annealing times. The Cu-rich regions formed during annealing (Fig. 3c–f) also have a decrease in Zr content, consistent with previous observations of segregation of these species during low temperature annealing in both thin film [13] and bulk [21] ZCAN. Furthermore, the requirement for the displacement of Ni preceding surface oxidation is consistent with previous observations that increasing Ni content in ZCAN BMG leads to increased oxidation resistance [22].

The onsets of the Cu- and Ni-rich regions correlate well with the formation of the surface oxide layer. As seen in Fig. 4b, the oxide thickness is seen to increase significantly from 2 to 15 nm after annealing for 5 to 30 min, respectively, and then increases only slightly (to 17 nm) after annealing for 120 min. Previous investigations of ZCAN BMG suggest surface oxidation follows a parabolic rate law for the conditions used in this study [23]. A dashed line is shown in Fig. 4b corresponding to the parabolic diffusion length, $d = \sqrt{4Dt}$, where D is the diffusion coefficient, and t the diffusion time. A good fit was achieved to the experimental data for annealing times between 0 and 30 min using $D = 2.9 \times 10^{-20}$ m^2/s, which is approximately one order of magnitude higher than what has been measured for Ni diffusion in ZCAN BMG ($D \approx 3 \times 10^{-21}$ m^2/s) [24]. The relatively close agreement between oxide growth and experimentally measured diffusivities suggests that the surface oxidation is initially limited by the back-diffusion of Ni and/or Cu as proposed in previous studies of ZCAN BMG [23]. It should be noted that the diffusion length corresponding to $D = 2.9 \times 10^{-20}$ m^2/s and t = 60 min (d = 20 nm) is consistent with the size of the majority of oxidized (dark) regions observed in top-down HAADF analysis (Fig. 1c) suggesting lateral oxidation may also be controlled by the diffusion of Ni and/or Cu laterally in the film.

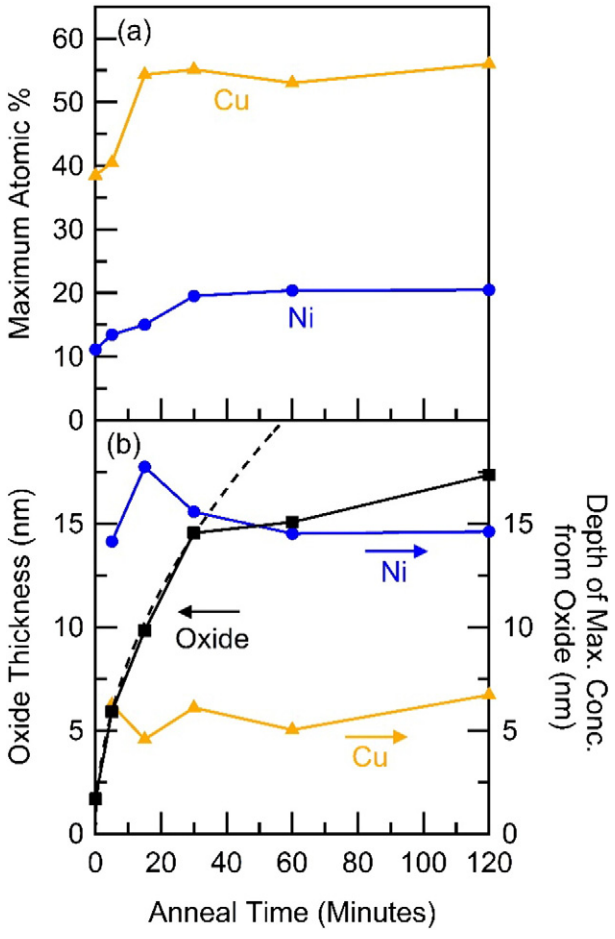

Fig. 4. Analysis of XPS depth profiles for ZCAN thin films annealed at 300 °C. (a) Maximum relative atomic concentrations of Cu and Ni. (b) Surface oxide thickness and distance of maximum concentrations from surface oxide. The dashed line corresponds to the diffusion length $d = \sqrt{4Dt}$ for $D = 2.9 \times 10^{-20}$ m^2/s.

Between 30 and 120 min annealing the growth in oxide thickness deviates from a parabolic form suggesting further oxidation may be limited by diffusion of a more slowly moving component, such as Zr. The oxide growth between 30 and 120 min can be well approximated by a linear relationship ($R^2 = 0.98$) yielding an oxide growth rate of 0.032 nm/min. This growth rate is consistent with a previous study on the oxidation of Zr metal [25]. In the previous study, Zr oxidation could be separated into an initial fast growth regime followed by a much slower, approximately linear growth regime. For 300 °C this transition occurred near t ≈ 40 min and the growth rate for t > 40 min was approximately 0.030 nm/min [25]. Both the time of transition and the subsequent growth rate are in close agreement with the present study, suggesting that oxide growth at longer anneal times (30 to 120 min) may be controlled by the outward diffusion of Zr.

An additional explanation for the observed oxidation behavior can be given based on theories of electric-field controlled oxide growth during initial stages of annealing [26]. That is, a potential difference is formed across the oxide layer between surface adsorbed oxygen and the underlying metal and this built-in electric field drives cation diffusion (in this case, primarily Zr) through the oxide promoting growth. The driving force for such growth involves electron tunneling through the oxide layer which decreases exponentially with distance leading to a critical thickness where a significant drop in oxide growth is observed [25]. The larger oxide thickness in the present study following the initial (fast) growth (≈15 nm) compared to the previous study on Zr metal (≈2.5 nm) could be explained in part by the lower oxygen pressure used in the previous study ($pO_2 = 2 \times 10^{-6}$ Pa) and/or the different metal composition [25]. For example, the buildup of Cu observed in the present study during initial stages of growth may lead to an increased concentration of mobile electrons at the oxide/metal interface thus increasing the terminal thickness for electric-field driven growth [26].

We now summarize our observations on the compositional inhomogeneities observed during the initial stages of thermal oxidation of ZCAN thin films in air. Annealing at a temperature of 300 °C results in the migration of the majority of the oxygen incorporated during deposition out of the bulk of the ZCAN film even for short times (5 min). Simultaneously, the thin native oxide layer begins to grow in thickness. Initially, Zr and Al metal are available at the film surface leading to oxide formation limited by the back-diffusion of Cu and Ni, resulting in fast oxide growth for t < 30 min. The growth in this regime may be further enhanced by migration of Zr cations to the oxide surface via the electric field established across the thin oxide layer. The displacement of Cu and Ni leads to an enrichment of these species at the oxide-film interface. Ni is displaced more readily due its increased diffusivity relative to Cu [27], resulting in a buildup adjacent to the oxide layer. Cu is displaced more slowly, and the strong immiscibility of Cu and Ni causes Cu accumulation above the Ni-rich region. At longer times (t ≥ 30 min) the majority of Zr metal near the film surface has undergone oxidation and further growth becomes limited by the outward diffusion of Zr, leading to a decreased growth rate that is consistent with oxidation of Zr metal [25]. The formation of a ZrO_2 surface layer on top of a Cu rich layer has been observed previously for freely solidified surfaces of Cu–Zr amorphous alloys and after extended exposures to ambient conditions (in laboratory air and dry air for 34 months) [28]. It was proposed that upon oxidation that a dense ZrO_2 layer forms,

and as the Zr metal is consumed through oxidation a copper rich layer forms underneath. Since these studies were performed at room temperature no significant growth of the ZrO_2 layer was seen for the time interval investigated.

4. Conclusions

Thermal oxidation of ZCAN amorphous metal thin films for short times (<60 min) and moderate temperatures (300 °C) results in significant compositional inhomogeneities in both vertical and lateral directions. We have found that the films remain amorphous irrespective of the oxidation conditions used in these studies. The incorporation of oxygen during deposition may help stabilize the amorphous phase of the film, however we find that oxygen is highly mobile even during the very initial stages of annealing. The rapid diffusion of oxygen in ZCAN films may potentially lead to instabilities in both material and device properties. The initial stages of surface oxidation are consistent with prior studies on bulk metallic glass, however we have shown that the unique boundary conditions present in thin films lead to distinct differences in the oxidation properties of ZCAN thin films. This detailed investigation into the role of diffusion of each metal species has provided insight into processes governing initial stages of surface oxidation, which is expected to aid in determining the suitability of ZCAN thin films for several emerging applications.

Acknowledgments

This research is funded through the Center for Sustainable Materials Chemistry, which is supported by the U.S. National Science Foundation under Grant CHE-1102637.

References

[1] A. Inoue, Stabilization of metallic supercooled liquid and bulk amorphous alloys, Acta Mater. 48 (2000) 279–306.
[2] J. Eckert, N. Mattern, M. Zinkevitch, M. Seidel, Crystallization behavior and phase formation in Zr–Al–Cu–Ni metallic glass containing oxygen, Mater. Trans. JIM 39 (1998) 623–632.
[3] J.P. Chu, J.S.C. Jang, J.C. Huang, H.S. Chou, Y. Yang, J.C. Ye, Y.C. Wang, J.W. Lee, F.X. Liu, P.K. Liaw, Y.C. Chen, C.M. Lee, C.L. Li, C. Rullyani, Thin film metallic glasses: unique properties and potential applications, Thin Solid Films 520 (2012) 5097–5122.
[4] P. Sharma, W. Zhang, K. Amiya, H. Kimura, A. Inoue, Nanoscale patterning of Zr–Al–Cu–Ni metallic glass thin films deposited by magnetron sputtering, J. Nanosci. Nanotechnol. 5 (2005) 416–420.
[5] P. Sharma, N. Kaushik, H. Kimura, Y. Saotome, A. Inoue, Nano-fabrication with metallic glass — an exotic material for nano-electromechanical systems, Nanotechnology 18 (2007) 6.
[6] C.L. Chiang, J.P. Chu, F.X. Liu, P.K. Liaw, R.A. Buchanan, A 200 nm thick glass-forming metallic film for fatigue-property enhancements, Appl. Phys. Lett. 88 (2006) 3.
[7] E.W. Cowell, C.C. Knutson, J.F. Wager, D.A. Keszler, Amorphous metal/oxide nanolaminate, ACS Appl. Mater. Interfaces 2 (2010) 1811–1813.
[8] E.W. Cowell, C.C. Knutson, N.A. Kuhta, W. Stickle, D.A. Keszler, J.F. Wager, Engineering anisotropic dielectric response through amorphous laminate structures, Phys. Status Solidi (a) 209 (2012) 777–784.
[9] E.W. Cowell, N. Alimardani, C.C. Knutson, J.F. Conley, D.A. Keszler, B.J. Gibbons, J.F. Wager, Advancing MIM Electronics: Amorphous Metal Electrodes, Adv. Mater. 23 (2011) 74-+.
[10] B. Tulu, W.Z. Chang, J.P. Chu, S.F. Wang, Forming-free resistive switching characteristics of 15 nm-thick multicomponent oxide, Appl. Phys. Lett. 103 (2013) 5.
[11] J. Schroers, G. Kumar, T.M. Hodges, S. Chan, T.R. Kyriakides, Bulk metallic glasses for biomedical applications, JOM 61 (2009) 21–29.
[12] N. Kaushik, P. Sharma, S. Ahadian, A. Khademhosseini, M. Takahashi, A. Makino, S. Tanaka, M. Esashi, Metallic glass thin films for potential biomedical applications, J. Biomed. Mater. Res. B Appl. Biomater. 102 (2014) 1544–1552.
[13] L. He, J.P. Chu, C.L. Li, C.M. Lee, Y.C. Chen, P.K. Liaw, P.M. Voyles, Effects of annealing on the compositional heterogeneity and structure in zirconium-based bulk metallic glass thin films, Thin Solid Films 561 (2014) 87–92.
[14] S.W. Muir, E.W. Cowell, W. Wang, J.F. Wager, D.A. Keszler, Effects of oxygen incorporation on the physical properties of amorphous metal thin films, J. Phys. Chem. C 118 (2014) 9647–9651.
[15] A. Gebert, J. Eckert, L. Schultz, Effect of oxygen on phase formation and thermal stability of slowly cooled Zr65Al7.5Cu7.5Ni10 metallic glass, Acta Mater. 46 (1998) 5475–5482.
[16] Z.P. Lu, C.T. Liu, Role of minor alloying additions in formation of bulk metallic glasses: a review, J. Mater. Sci. 39 (2004) 3965–3974.
[17] A. Dhawan, V. Zaporojtchenko, F. Faupel, S.K. Sharma, Study of air oxidation of amorphous Zr65Cu17.5Ni10Al7.5 by X-ray photoelectron spectroscopy (XPS), J. Mater. Sci. 42 (2007) 9037–9044.
[18] A. Dhawan, S.K. Sharma, Role of alloying elements during high temperature oxidation of bulk amorphous alloy Zr65Cu17.5Ni10Al7.5 in air, Indian J. Pure Appl. Phys. 41 (2003) 453–456.
[19] K. Asami, M. Kikuchi, K. Hashimoto, An auger electron spectroscopic study of the corrosion behavior of an amorphous Zr40Cu60 alloy, Corros. Sci. 39 (1997) 12.
[20] S.K. Sharma, T. Strunskus, H. Ladebusch, F. Faupel, Surface oxidation of amorphous Zr(65)Cu(17.5)Ni(10)Al(7.5) and Zr(46.75)Ti(8.25)Cu(7.5)Ni(10)Be(27.5), Materials Science and Engineering a-Structural Materials Properties Microstructure and Processing 304 (2001) 747–752.
[21] N. Van Steenberge, A. Concustell, J. Sort, J. Das, N. Mattern, A. Gebert, S. Surinach, J. Eckert, M.D. Baro, Microstructural inhomogeneities introduced in a Zr-based bulk metallic glass upon low-temperature annealing, Mater. Sci. and Eng. a-Struct. Mater. Properties Microstructure and Process. 491 (2008) 124–130.
[22] Y. Wu, G.M. Song, T. Nagase, Y. Umakoshi, Effect of Ni-addition on the crystallization behavior and the oxidation resistance of Zr-based metallic glasses below the crystallization temperature, J. Non-Cryst. Solids 357 (2011) 1136–1140.
[23] A. Dhawan, K. Raetzke, F. Faupel, S.K. Sharma, Air oxidation of Zr65Cu17.5Ni10Al7.5 its amorphous and supercooled liquid states, studied by thermogravimetric analysis, Phy. Stat. Solidi A-Appl. Mater. Sci. 199 (2003) 431–438.
[24] K. Knorr, M.-P. Macht, H. Mehrer, Self-diffusion in bulk metallic glasses, Materials Research Society 1998, pp. 269–274.
[25] A. Lyapin, L.P.H. Jeurgens, E.J. Mittemeijer, Effect of temperature on the initial, thermal oxidation of zirconium, Acta Mater. 53 (2005) 2925–2935.
[26] N. Cabrera, N.F. Mott, Theory of the oxidation of metals, Rep. Prog. Phys. 12 (1949) 22.
[27] H. Hahn, R.S. Averback, H.M. Shyu, Diffusion studies in amorphous NiZr alloys and their relevance for solid-state amorphizing reactions, J. Less-Common Met. 140 (1988) 345–352.
[28] K. Asami, M. Kikuchi, K. Hashimoto, An auger electron spectroscopic study of the corrosion behavior of an amorphous $Zr_{40}Cu_{60}$ alloy, Corrosion 39 (1997) 95–106.